Sustainable Geosciences: People, Planet and Prosperity 1 (2025) 100006

Contents lists available at ScienceDirect

Sustainable Geosciences: People, Planet and Prosperity

journal homepage: www.elsevier.com/locate/susgeo

A global downstream approach to mapping surface urban heat islands using open data and collaborative technology

Chiara Richiardi [a,b,c,*], Letizia Caroscio [c,d,**], Edoardo Crescini [c,e,f], Massimo De Marchi [e,f], Giovanni Marco De Pieri [c], Christopher Ceresi [c], Federico Baldo [c,g], Matteo Francobaldi [c,h], Salvatore Eugenio Pappalardo [e,i]

[a] Italian National Agency for New Technologies, Energy and Sustainable Economic Development (ENEA), Saluggia (VC), Italy
[b] University of Torino, Department of Life Sciences and Systems Biology (DBIOS), Italy
[c] SCIFT, Laboratory of Science, Climactivism, Imagination, Fostering Knowledge and Technology, Bologna, Italy
[d] University of Bologna, Department Civil, Chemical, Environmental and Materials Engineering (DICAM), Italy
[e] University of Padova, Department Civil Environmental and Architectural Engineering (ICEA), Italy
[f] Centre of Excellence Jean Monnet on Just Fossil Fuel Transition, Department Civil Environmental and Architectural Engineering (ICEA), University of Padova, Italy
[g] Sorbonne Université, Institute Pierre Louis d'Épidémiologie et de Santé Publique (INSERM), France
[h] University of Bologna, Department Informatics - Science and Engineering (DISI), Italy
[i] GIScience for Humanity, Urban Space and the Biosphere (GIShub Padova)

ARTICLE INFO

Keywords:
Surface Urban Heat Island
EO downstream
Remote sensing
Urban planning
Dissemination
Open data & technology
Digital divide
Data democratization
Science-activism

ABSTRACT

This paper presents a fully automated, open-source workflow for mapping and analysing Surface Urban Heat Island Intensity (SUHII) in urban areas. The method integrates freely available Earth Observation datasets, including Landsat imagery and SRTM elevation data, and ensures generalizability across diverse landscapes by analysing homogeneous altitudinal zones. This avoids over- or underestimation of thermal anomalies due to elevation differences. The pipeline requires only a city name and a local folder path as inputs, producing standardized warm-season Land Surface Temperature and SUHII maps in GeoTIFF format with full metadata. Developed in modular R and Python environments, the code supports easy adaptation, dataset integration, and deployment in web or desktop applications. Designed to lower technical barriers, the platform merges technical and experiential knowledge through citizen participation, enabling non-experts to explore urban thermal anomalies and their social and health implications. This approach fosters equitable climate adaptation and environmental justice by making climate-relevant spatial data accessible and actionable for citizens, researchers, and decision-makers.

1. Introduction

Heatwaves (HWs) have become the "daily face" of climate change, shaping the global "collective imagery" of how extremes impact vast areas of the Earth, particularly densely urbanized regions (Moreno et al., 2010; WMO, 2022). Furthermore, the impacts of HWs strongly amplify the increase of urban temperatures through a positive feedback loop on the effect of Urban Heat Island (UHI). This phenomenon is defined as the localized thermal anomalies compared to the rural surrounding temperatures. UHIs are mainly driven by factors of the city features and characteristics: size, land use, albedo and urban morphology (Oke, 1973; Santamouris, 2020; Javanroodi et al., 2021, 2022). The combined impacts of HWs and UHIs dramatically raise heat-related risks, as shown in Europe where summers 2022 and 2023 caused 61,672 and 47,690 excess deaths (Ballester et al., 2023).

Recent projections highlight that the probability and intensity of HWs in Europe will rise significantly under different global warming levels. Using bias-corrected daily data from CMIP6 multi-model ensembles, studies show that at 2.0 °C of global warming compared to 0.5 °C, the annual number of HW days could increase three- to fourfold in northern Europe and more than sixfold in southern regions, with extremity indices rising up to tenfold. Moreover, HWs with a return period

* Corresponding author at: Italian National Agency for New Technologies, Energy and Sustainable Economic Development (ENEA), Saluggia (VC), Italy.
** Corresponding author at: SCIFT, Laboratory of Science, Climactivism, Imagination, Fostering Knowledge and Technology, Bologna, Italy.
E-mail addresses: chiara.richiardi@enea.it (C. Richiardi), letizia.caroscio2@unibo.it (L. Caroscio).

https://doi.org/10.1016/j.susgeo.2025.100006
Received 24 July 2025; Received in revised form 24 October 2025; Accepted 27 October 2025
Available online 28 October 2025

of 10 years at 0.5 °C warming would become almost biennial in northern Europe (≈50 % annual probability) and nearly annual in southern Europe (80–90 %). Even the most extreme 100-year events would reach probabilities close to 20 % in the north and 60 % in the south, underscoring the urgency of addressing UHIs within a rapidly warming European climate context (Ruosteenoja and Jylhä, 2023).

Vulnerability to HW and UHI impacts is evident in Euro-Mediterranean countries, critical Asian regions (Nepal, Pakistan, Bangladesh), parts of the U.S. (Arizona, Texas, California), Latin America, Nort East of Brazil, Guyana, Coastal Perù, but also Amazon Region, and African nations such as Botswana, Namibia, Mozambique, Zambia, and South Africa (Lauwaet et al., 2024; Roshan et al., 2024). A global LST analysis (2003–2020) shows urban heat levels doubled, with anomalies exceeding 10 °C compared to surrounding areas (Mentaschi et al., 2022).

Extreme events expose not only the physical dynamics of climate change but also the unequal distribution of its impacts across scales, countries, and municipalities, worsening social class inequalities. These impacts vary according to political, economic, and socio-cultural contexts. Over the past decade, academia and civil society have increasingly called for climate justice to be integrated into risk assessment and adaptation planning, fuelling global debates (Gardiner, 2011; Bulkeley et al., 2013, 2014; Robinson and Shine, 2018; Porter et al., 2020; Cañizares et al., 2024; Rigon, 2025; Ruiz de Gopegui et al., 2025). As widely documented, impacts of HWs amplify pre-existing social inequalities, by disproportionately affecting the most vulnerable populations including the elderly, children, low-income families, women, migrants, and ethnic minorities (Voelkel et al., 2018; Anguelovski et al., 2024). For instance, heat-related morbidity and mortality has been found significantly higher in marginalized and underserved neighbourhoods, where the most vulnerable social groups are affected by stronger intensity of UHI (Meenar et al., 2023; Eyni et al., 2025; Grislain-Letrémy et al., 2025; Ho et al., 2025).

This study responds to the growing need for inclusive, data-informed approaches to urban climate resilience by aligning with multiple United Nations Sustainable Development Goals (SDGs) (United Nations, 2015). By automating the mapping of Surface Urban Heat Island Intensity (SUHII) using globally available data and reproducible methods, the proposed workflow supports SDG 11 (Sustainable Cities and Communities) and SDG 13 (Climate Action) by enabling equitable monitoring of urban thermal anomalies and informing adaptive planning strategies (Avtar et al., 2020). It also contributes to SDG 3 (Good Health and Well-being) by facilitating the identification of heat-exposed communities, thus supporting efforts to reduce environmental health risks (Yuan, 2021). Through open access, transparency, and broad usability, the platform strengthens public accountability and inclusive decision-making (Bachmann et al., 2022), advancing SDG 16 (Peace, Justice and Strong Institutions). Finally, by fostering open-source collaboration and partnerships across scientific, institutional, and civic actors, the study reinforces the goals of SDG 17 (Partnerships for the Goals) (Bachmann et al., 2022). In this context, the issue of “where” extreme events impact, “where” vulnerable social groups are spatially distributed on the territory as well as “which and how” data are used are crucial to include the dimension of justice and equity in climate risk assessment and adaptation planning. UHI is a general term related to the temperature difference among urban and rural areas. However, according to the different approaches to detect and to assess this thermal phenomenon, different terms are adopted in scientific literature: at canopy-level UHI detection is based on near-surface air temperature (namely, CUHI); at surface UHI, temperature values are related to the three dimensions of the urban landscape such as ground, rooftops, and walls (SUHI) (Stewart and Mills, 2021). The calculation of UHI intensity at surface level (SUHII) is based on the thermal difference among urban and rural area (SUHII= ΔT_u-T_r where: T_u= urban surface temperature, T_r= rural surface temperature).

UHI can be investigated through three main methodological approaches, each offering distinct advantages in terms of spatial coverage, resolution, and accessibility. The first approach is based on direct measurements of air temperature, through a network of ground meteorological stations, providing real-time continuous data of the main weather variables (temperature, humidity, wind, rainfall); the second one is based on high-resolution analyses, downscaling data from climate models at grid size of 100 m (i.e. the UrbClim from VITO); the third one is based on the use of public data from thermal sensors to detect LST by remote sensing technologies and modelling, generally equipped on public satellite platforms and unmanned aerial vehicles. The latter approach is widely adopted as they are characterized by a global spatial continuity of LST values which are used as data proxy for mapping thermal anomalies (Zhou et al., 2018); moreover, the worldwide availability of freely accessible LST images from NASA (Landsat program) and Copernicus satellites (Sentinel-3), combined with modern GIS-based modelling tools, has made Surface Urban Heat Island (SUHI) mapping the most widely used and straightforward method for mapping and assessing the spatial distribution of SUHIs. Even if open-source geospatial technologies, data and software as well as GIS-based platforms are supported by international open-source communities, accessibility and usability of such geotools for mapping SUHI remain limited to experts or skilled citizens. The general aim of the present study is to democratize access to EO technologies and to increase the awareness of local climate extreme impacts from UHI on the urban territory and on public health by bridging the gap between science and citizens. The specific objectives aim i) to design, and validate a replicable, open methodology supported by a standardized workflow to automatically assess and to geovisualize, by a geographical location input worldwide, critical SUHI hotspots at urban scale; ii) to provide a complete open source, open technology and open data system for citizen awareness and engagement in local climate actions.

2. Study area

The research deals with mapping surface urban heat islands developing a global downstream approach using open data and collaborative technology. Despite not focusing on a specific study area the article is centered on the geographies of cities of all the world, and, nevertheless the limited space of the article, we presents the application of SUHI (Surface Urban Heat Island) in 40 cities of the world located in different latitudes, within a range which include the majority of climate typologies on Earth (from 61.2° N with Anchorage to 42.9° S with Hobart), and longitudes ensuring broad geographical coverage. The selection also accounted for population size, covering cities from small (e.g., Bendigo, Australia, ~121,000) and medium (e.g., Alicante, Spain ~359,000) to large (e.g., Belém, Brazil ~2.43 million) and mega-cities (e.g., Buenos Aires, Argentina ~15.6 million; Nanjing, China ~9.9 million).

3. Background

Being the cities the primary sites of vulnerability to climate extreme, in the age of proliferating Earth Observation (EO) technologies and Big Earth Data, as well as of the integration of Information and Communication Technology (ICT) infrastructures based on urban environmental sensor networks, cities have become primary sites also of data production and urban heat monitoring, draining important public investments to design and manage different adaptation strategies and measures. However, the most affected social groups are often scarcely represented both in UHI analyses, in data collection/visualization and decision-making processes. For instance, despite the increasing global availability of public climate data from authoritative sources (IPCC, Copernicus, NASA, NOAA, Climate Central but also national and local institutions), significant barriers to usability and inclusivity persist (Kumar et al., 2024; Bara, 2025), including data accessibility and data visualization, inaccessible platforms and data formats (Kim, 2023; Soden et al., 2025). Moreover, often datasets are limited to certain cities or regions, where

projects and investments are supporting climate policies and strategies.

In addition, the spread in the last years of different business-driven UHI mapping services, generally based on proprietary systems and closed algorithms, are making the access to the data platforms even more limited, generating a digital divide among countries and cities, worldwide. Among many available commercial platforms, wide market sectors are currently covered by ArcGIS Platform (ESRI), Environmental Insights Explorer (Google), IBM Environmental Intelligence (IBM), UHear (ARUP), and EarthPlatform (Descartes Lab). These platforms strongly rely on proprietary workflow, algorithms, and software, limiting transparency and broader accessibility compared to open-source and easy-of-use geospatial infrastructures. Such barriers, thus, limit the most vulnerable social groups from being informed and empowered into the climate change debate as well as directly engaged in climate decision-making and adaptation planning.

4. Data

This research strongly relies on data collected and processed; three main data sources were used (Table 1):

- Satellite imagery from Landsat 8 and 9,
- Digital Elevation Model,
- Land cover data derived from OpenStreetMap.

4.1. Landsat

The primary input for deriving LST and quality assurance (QA) information comes from the USGS Landsat Collection 2 Level 2 (C2 L2) Science Product (L2SP) dataset (Earth Resources Observation and Science (EROS) Center, 2020). Specifically, two types of bands are used: (1) Surface Temperature (ST) band 10 product allowing direct estimation of temperature values; (2) QA Pixel Band, which provides essential quality flags (e.g., cloud contamination, cloud shadow, and sensor anomalies), enabling a filtering of poor-quality pixels before LST calculation. Landsat scenes are selected to match the temporal window of interest for each study area, and to meet an optimal trade-off between radiometric quality and temporal coverage. To reduce the influence of cloud contamination, we tested four alternative thresholds of maximum cloud cover (20 %, 30 %, 50 %, and 70 %) for scene selection (Table S1). For each threshold, we quantified the proportion of usable scenes, the variability of warm-season aggregated surface temperature (LST), and the stability of summary statistics across cities. Lower thresholds (20 %) resulted in fewer available observations but more consistent LST values, whereas higher thresholds (70 %) maximized data availability at the cost of substantially increased variability and potential cold biases from cloud contamination. Based on this trade-off, we adopted a fixed 30 % cloud cover threshold as a compromise, ensuring sufficient temporal coverage while maintaining an acceptable level of data quality (Li et al., 2022; Yang et al., 2025).

4.2. Digital elevation model (DEM)

A DEM is used to account for topographic variation that may influence surface temperature estimates and for any ancillary spatial analyses. Both R and python implementations access DEM from the NASA's Shuttle Radar Topography Mission (SRTM), at 30 m of resolution (1 Arc-Second Global).

Table 1
Summary of data specifics. NA = Not Applicable.

Data	Coverage	Resolution (m)	Format
Landsat 8–9	Global	30	Raster
SRTM30	Global	30	Raster
OSM	Global	NA	Vector

4.3. OpenStreetMap (OSM)

OSM data are incorporated to further categorize land cover and retrieve administrative boundaries (OpenStreetMap contributors, 2025). Relevant layers include:

- Impervious areas: used to identify urbanized zones (e.g., roads, buildings, paved surfaces) for the characterization of surface heat retention.
- Rural areas: used to calculate the reference temperature that would characterize the specific area without artificial surfaces.
- Administrative boundaries of the municipality: facilitate spatial clipping over an administrative unit for the analyses. These are employed both to simplify the overall workflow and to ensure that outputs align with actual planning units. By clipping the analysis to well-defined administrative limits, the results can be directly interpreted and applied by local authorities and urban planners working within those jurisdictions.

These OSM layers are accessed via open-data APIs and represent a flexible, updatable source of community-driven geographic information. All vector data are converted into standardized coordinate reference systems matching those of the Landsat and DEM datasets to enable coherent spatial analysis.

5. Methods

The workflow was initially developed in R (R core team, 2024) to take advantage of widely available statistical and geospatial analysis libraries. At a later stage, the same workflow was implemented in Python (version 3.9) with the aim of simplifying its integration into web platforms and extending its adoption to a wider community of developers.

5.1. User's inputs and preliminary operations

Currently, the workflow (Fig. 1) takes two user-defined parameters: (1) the city of interest and (2) a local folder path. The system is designed to analyse the most recent full warm season depending on the hemisphere and the current date. To consistently identify the warm season across study areas with different climatic regimes, we implemented a rule-based approach grounded in the Köppen-Geiger climate classification (Rubel and Kottek, 2010) and the hemispheric location of each area of interest (AOI). First, the AOI corresponding Köppen-Geiger class is retrieved. Based on the extracted class and the hemisphere, a set of default warm months is, then, assigned following explicit climate-dependent rules. In tropical climates (A), rainforest regions (Af) were considered warm throughout the year, whereas for monsoonal (Am) and savanna (Aw) climates the warm season was restricted to the local dry period (November-April in the Northern Hemisphere, May-October in the Southern Hemisphere). In arid regions (B), the warm season was defined as April-September in the Northern Hemisphere and October-March in the Southern Hemisphere, ensuring coverage of the dry-hot months. In temperate regions (C), Mediterranean climates (Csa, Csb) were assigned April–September, while oceanic climates (Cfb, Cfc) were restricted to peak summer (June–August in the Northern Hemisphere, December-February in the Southern Hemisphere). Continental climates (D) were treated analogously, with warm months defined as June-August in the Northern Hemisphere and December-February in the Southern Hemisphere. Polar or undefined climates (E) were also restricted to these summer months.

Once the warm months were determined, the algorithm computed the corresponding start and end dates. To avoid incomplete seasons, if the current date fell before the end of the ongoing warm season, the time

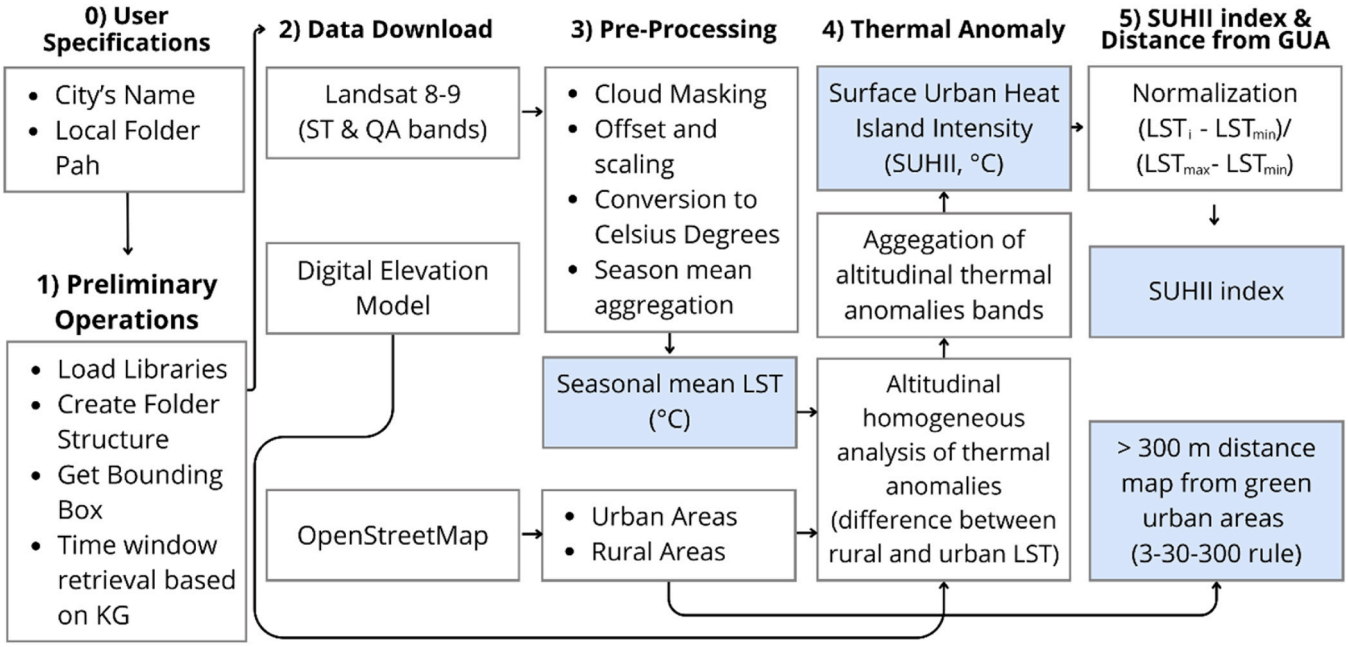

Fig. 1. Flowchart of the algorithm. Outputs are in the blue boxes. (KG = Köppen-Geiger).

window was shifted back one year, ensuring that only fully available seasons were considered. This procedure allowed us to automatically extract the last complete warm-season interval for each AOI in a manner consistent across climates and hemispheres, while explicitly accounting for warm-season asymmetries between Northern and Southern Hemisphere sites This approach is driven by two main considerations. First, the reliability of LST: by collecting multiple images across a season, the workflow computes an average LST over multiple scenes, helping to mitigate the effects of cloud cover and other transient atmospheric factors. This yields more consistent and robust surface temperature estimates. Secondly, the timely data integration: because OSM layers provide the most recent land cover information, restricting the analysis to the latest complete season ensures alignment between up-to-date ground features and the corresponding satellite imagery, maintaining coherence between surface temperature observations and on-the-ground conditions. Preliminary operations include installing and loading the necessary packages and creating the folder structure (Figure S1) in the local folder previously set up. More detail in the Supplementary materials.

5.2. Data retrieval

The workflow retrieves and download automatically all the required input data. First, it retrieves the bounding box of the municipality defined by the user through OSM. Secondly, inside the bounding box, other queries are performed with specific key–value combinations (Figure S2), to get administrative boundaries, rural areas, and impervious areas. Polygons and multi-polygons are extracted for each feature and aggregated into a single shapefile, which are saved locally. Then, it downloads a DEM, with 30-meter resolution, covering the city of interest. Finally, the ST and QA bands of each scene (1) falling within the period of analysis and (2) with a cloud cover under the threshold (30 %) are downloaded via the USGS M2M API. Further details can be found in the SM.

5.3. Pre-processing

Once the Landsat dataset is downloaded, each surface temperature (ST) band undergoes a series of pre-processing steps. First, the image is clipped to the bounding box of the area of interest, and any invalid pixels are masked according to the corresponding QA band. Next, the scaling factor (0.00341802) and additive offset (149), following Landsat C2 L2 guidelines, (Earth Resources Observation and Science (EROS) Center, 2024) are applied, followed by unit conversion from Kelvin to Celsius using:

$$LST = ((ST \times 0.00341802) + 149) - 273.15$$

where ST denotes the surface thermal band, and LST is the resulting land surface temperature (in °C).

Individual LST scenes are aggregated to produce a single warm-season mean LST image. All vector shapefiles (e.g., land cover and administrative boundaries) are rasterized, and all layers, including the DEM, are reprojected and resampled to match the extent and the spatial resolution of the LST data. To characterize the temporal stability of LST, we computed two complementary pixel-wise variability metrics from the raster stack of LST scenes: the standard deviation (SD) and the interquartile range (IQR). The SD provides a direct measure of dispersion around the mean and is widely used to assess spatiotemporal variability in remote sensing time series (Charpentier and Groffman, 1992). The IQR, defined as the difference between the 75th and 25th percentiles, offers a robust alternative that reduces the influence of extreme values or residual noise in the LST signal (Zhang et al., 2018; Knott et al., 2023). Both metrics were mapped to highlight areas of relatively stable versus highly variable LST conditions over the study period.

5.4. Land surface temperature anomalies and indices

To map SUHII as surface thermal anomalies relative to the average temperature of surrounding natural and rural areas, the tool proceeds by extracting the average LST of rural areas, selecting only the pixels at a distance greater than 300 m from man-made areas, to avoid their thermal influence and thus obtain a more robust estimate, as applied in other studies (Pappalardo et al., 2023). This is the reference temperature of the specific geographical context of the study area, which is then subtracted from the average LST, previously calculated, obtaining the thermal anomaly or the Surface Urban Heat Island Intensity (SUHII) map.

$$SUHII = LST_i - \quad LST_{rural}$$

where LST_i represents the LST of a pixel in a specific image and LST_{rural} is the reference LST, calculated as average value of the surrounding rural areas.

To simplify the interpretation of the map, as well as the possibility of an immediate comparability between different study areas, the SUHII values are normalized (Zargari et al., 2024), producing a dimensionless $SUHII_{index}$ map ranging from 0 to 1:

$$SUHII_{index} = (LST_i - LST_{\min})/(LST_{\max} - LST_{\min})$$

where, LST_i represents the LST of a pixel in a specific image, while LST_{max} and LST_{min} denote the maximum and minimum values of LST, respectively, for the same image as that of LST_i.

Pixels with $SUHII_{index}$ values close to 1 indicate stronger thermal anomalies, whereas those near 0 suggest little to no heat anomaly.

Before the SUHII and $SUHII_{index}$ calculations, the topography of the study area is assessed. If the elevation range is less than 100 m, a single analysis is carried out. Otherwise, the workflow segments the study area into 100 m altitude bands, performing separate calculations for each band. This produces a series of SUHI and $SUHII_{index}$ maps, which are subsequently merged into a single output. By dividing the study area into homogeneous altitude classes, this approach uniquely accounts for the fact that LST, like air temperature, varies with elevation (Mutiibwa et al., 2015; Zargari et al., 2024). Consequently, it minimizes the risk of over- or underestimation, promoting a more accurate measurement of the SUHI phenomenon across diverse topographic conditions, ensuring consistency and applicability across any study area.

Optionally, the workflow includes a distance analysis that identifies all locations more than 300 m from urban green areas. This procedure produces an additional geospatial layer that, when used in conjunction with the SUHI map, enables planners and decision-makers to pinpoint neighbourhoods with reduced access to green space. By highlighting areas potentially in greater need of vegetation-based mitigation strategies, this feature supports evidence-based urban planning aimed at alleviating heat island effects and enhancing community well-being (Nieuwenhuijsen et al., 2022).

5.5. Validation of the altitude banding approach

To assess whether the 100 m elevation banding adequately accounts for orographic effects on LST, we validated it against a lapse-rate correction. The lapse rate describes the rate at which surface temperature decreases with altitude (°C per km), and provides a physically based reference for correcting temperature differences across elevations. For each study city, we first estimated the local lapse rate by regressing rural pixel LST against elevation. The resulting slope was used to adjust all pixel temperatures to a common reference altitude, chosen as the median rural elevation of the city of interest. We then recomputed SUHI from the lapse-rate-corrected data. Finally, these lapse-rate-corrected SUHI values were compared with those derived from the 100 m altitude banding. This procedure allowed us to evaluate whether the simpler banding scheme yields results consistent with a physically grounded lapse-rate correction.

6. Results

6.1. Outputs

The algorithm returns four outputs:

(1) the warm-seasonal LST mean, in °C, i.e. the warm-season mean aggregation of the available LST scenes' valid pixels,
(2) the metrics SD and IQR, in °C, to provide stability metrics,
(3) the thermal anomaly intensity (or SUHII) map, in °C, i.e. the absolute temperature anomalies between the urban and the surrounding rural areas,
(4) the $SUHII_{index}$ map, 0 – 1, dimensionless, i.e. the normalized value of the thermal anomaly intensity (Fig. 2),
(5) the distance from the green urban areas, in meters, i.e. the pixels with a greater distance then 300 m from urban green areas.

All maps are exported locally in GeoTIFF format, compliant with Open Geospatial Consortium (OGC) standards, and accompanied by metadata files that detail data sources, parameter settings, and processing methods. This ensures broad interoperability with common GIS software and facilitates reproducibility and data sharing.

6.2. Urban heat vulnerability

Cities exhibit markedly different responses to the ongoing climate crisis, as evidenced by variations in mean urban thermal anomaly over the 2024 warm season values of cities across the world (Fig. 3). When stratified by latitude band, extreme high-latitude cities (60°– 90° N/S) experience very low ambient temperatures, extreme seasonal sunlight variation (polar night/day), low humidity, and predominantly snowfall; these factors collectively attenuate the SUHI effect. Mid-latitude cities (30°– 60° N/S), whose climate exhibits four distinct seasons, moderate diurnal and seasonal temperature ranges, and relatively uniform precipitation, often developed within a green landscape context, display the greatest SUHI anomalies and are particularly vulnerable to heatwave events, both climatically and due to the inadequate adaptation of buildings stock. In contrast, low-latitude cities (0°–30° N/S) endure high temperatures year-round, pronounced wet and dry seasons, and influences from the humid equatorial belt or subtropical deserts; here, traditional urban morphology and architectural designs have historically mitigated heat stress, resulting in comparatively stable SUHI levels despite persistently warm conditions (Al Echcheikh El Alaoui, 2025; Stracqualursi, 2025).

Importantly, differences in urban form amplify these climatic contrasts. Low-latitude cities such as Marrakech are typically characterized by compact layouts with dense, narrow streets, high building proximity, and vernacular features such as courtyards, thick walls, and shaded passages. These forms enhance shading, ventilation, and passive cooling, thereby dampening the SUHI effect (Al Echcheikh El Alaoui, 2025; Stracqualursi, 2025). By contrast, many high- and mid-latitude cities, particularly in North America and parts of Europe, expanded with sprawling, low-density development patterns, larger surface parking areas, and more exposed building envelopes. Such morphologies increase surface heat absorption, reduce shading, and exacerbate urban heat retention, with clear links between urban sprawl and greater vulnerability to extreme heat (Stone et al., 2010). The comparative evidence thus suggests that compact, climate-responsive urban fabrics in low-latitude contexts tend to moderate thermal anomalies, whereas sprawling urbanism in mid- and high-latitude settings amplifies them.

This thermal behaviour gradient clearly emerges from Fig. 3, where cities located in highest latitudes, i.e. cold climate, such as Hobart, Anchorage, Bendigo, Adelaide among the others, are not exposed to heavy SUHI intensity. Mid-latitude cities, Nanjing, Nashville, Matsumoto and Kuala Lumpur, Belem, Dolisie, show the highest thermal discomfort of urban areas. Finally, low latitudes, like Marrakech and Hapur, experience even lower temperatures inside the urban areas compared to the surrounding rural areas. Notably, a subset of cities, including Phoenix, Kabul, and Lusaka, deviate from this expected latitudinal pattern. Their anomalous behaviour can be attributed to their environmental settings in torrid climates, where extreme aridity results in minimal thermal differentiation between urban and surrounding rural areas. This evidence points to three key implications. First, any comparative analysis of urban heat islands must explicitly account for climatic differentiation, for instance, through classifications such as

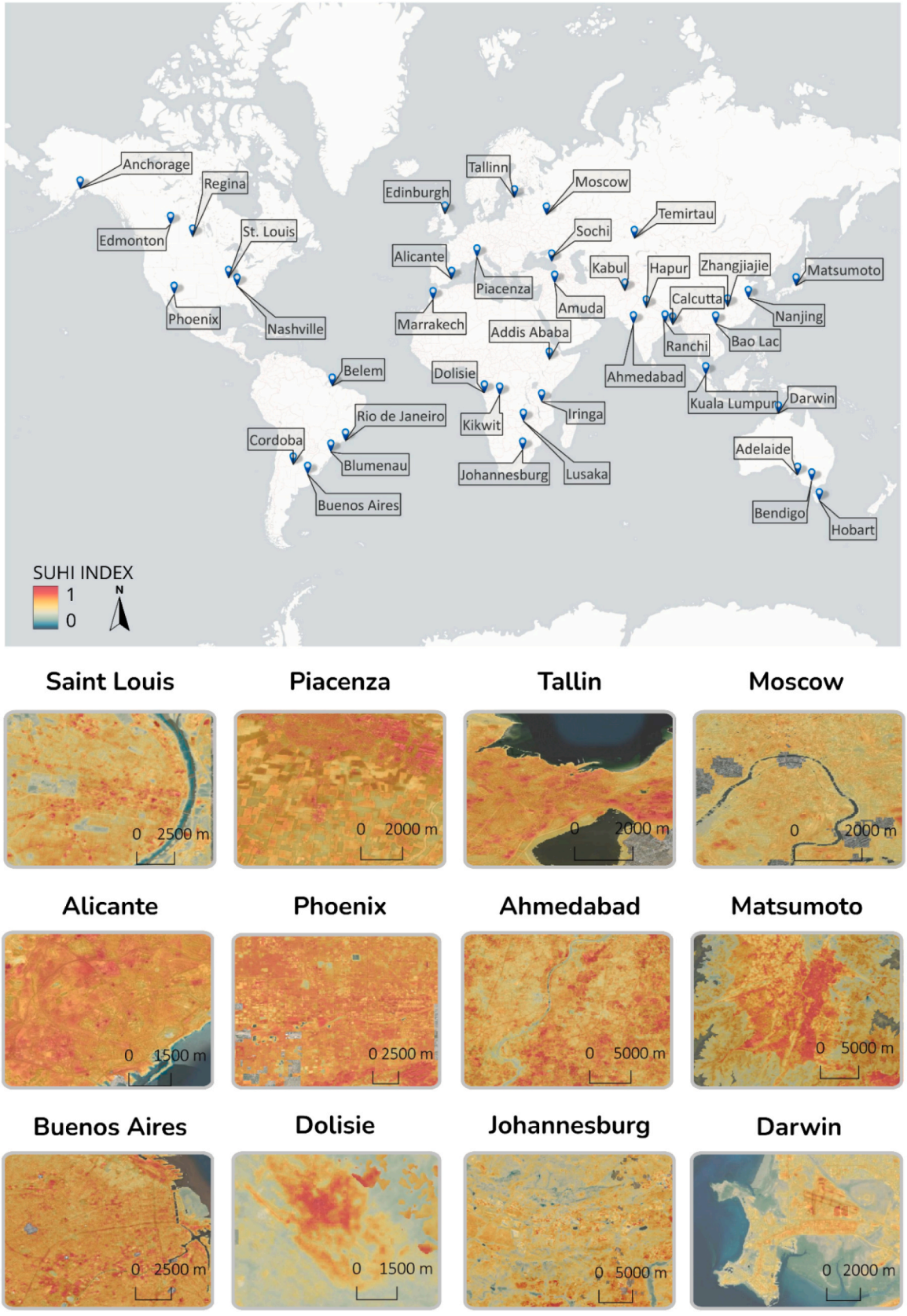

Fig. 2. Localization of the 40 cities used for testing the workflow and close-up of SUHII mapping examples globally, based on the warm season of 2024. Map reference system in the figure EPSG:3857.

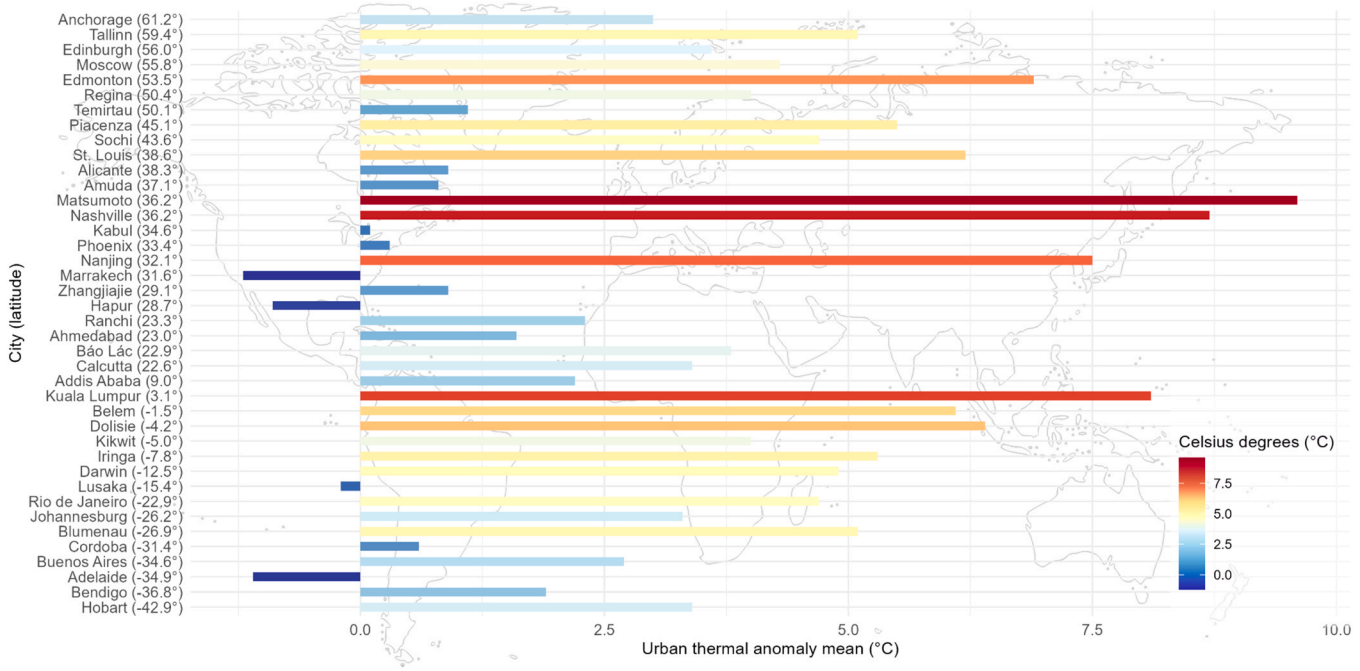

Fig. 3. Mean urban thermal anomaly across cities of the world, ordered by latitude, based on the warm season of 2024.

Köppen-Geiger, since background climate strongly conditions the magnitude and expression of the SUHI effect. Second, mid-latitude cities emerge as the least prepared for future climatic challenges, given both their high SUHI intensities and the structural limitations of their built environments. Third, in addition to supporting the mapping of heat islands at the individual city scale, the proposed approach enables systematic comparisons among cities within comparable climatic contexts. When cities are compared within comparable climatic contexts, the proposed approach can reveal those performing better or worse than expected. This provides a valuable basis for evaluating the effectiveness of adaptation and mitigation strategies, and for identifying both best-practice examples and critical cases requiring urgent policy intervention.

6.3. Validation of SUHI calculation for altitude bands

The thermal anomaly analysis through an altitudinal bending approach was validated by comparing the 100 m segmentation against a lapse-rate approach, in six of the 40 cities selected for the altitudinal range, i.e. Addis Ababa, Anchorage, Johannesburg, Matsumoto, Piacenza and Zhangjiajie. Across the six test cities, the elevation-band method closely matched the lapse-rate corrected SUHII (Figure S3). In five cities (Addis Ababa, Anchorage, Johannesburg, Piacenza, Zhangjiajie) the mean bias was within ±0.20 °C (0.01, −0.18, 0.10, −0.05, −0.15 °C, respectively), slopes spanned 0.93–0.99, and coefficients of determination were high (R^2 = 0.90–0.98). RMSEs in these cases were ≤ 1.39 °C (0.43–1.39 °C). Intercepts were small (−0.20–0.13 °C), indicating minimal constant offset between methods. Johannesburg showed the strongest agreement (bias = 0.10 °C, RMSE = 0.43 °C, slope = 0.99, R^2 = 0.98). Matsumoto was the only clear outlier, with a larger negative bias (−0.89 °C), higher error (RMSE = 2.62 °C), and a compressed regression slope (0.71; R^2 = 0.85), indicating reduced dynamic range of the banded product relative to the lapse-corrected reference. Bias confidence intervals were extremely narrow in all cases, consistent with the very large pixel samples used. Overall, these results support the use of the 100 m banding approach as a practical and robust proxy for lapse-rate correction across diverse cities.

6.4. Algorithm's performance

The algorithm was tested on a Windows 11 Pro machine with 32 GB of RAM and AMD Ryzen 7 2700X Eight-Core Processor 3.70 GHz. We tested the workflow over 40 cities worldwide, collecting processing time, allocated memory and data sizes (Table S2). The end-to-end processing pipeline required on average 11 ± 18 min and consumed 17 ± 45 GB of RAM per city, ranging from 4 min (Báo Lác, Vietnam) to 120 min (Moscow, Russia). Of the total runtime, the bulk was spent downloading satellite and vector data (Landsat: 4.56 ± 3.69 min; OSM: 4.57 ± 7.95 min), whereas core geospatial computations, i.e. LST derivation (0.53 ± 1.79 min), thermal anomaly & SUHII calculation (1.34 ± 6.44 min), and distance measures (≈0.01 min), were lightweight (Figure S5). The mean area processed was 2163 ± 3340 km^2, with 45 ± 28 % of downloaded Landsat scenes retained after cloud and footprint filtering. Downloading and handling DEM were reproducibly fast (< 0.5 min), but all metrics exhibited high variability across city extents. The input data download time required is weakly correlated to the area of the city processed (Figure S6), because it depends on how the layers are mapped in OSM: e.g. whether artificial surfaces are represented as aggregated neighbourhood polygons or as individual building footprints has a deep impact on the resulting dataset size. The average outputs' size is approximately around 8 MB (±13 MB).

7. Discussion

7.1. Heatwaves and climate extremes: from data democracy to climate justice

The thermal anomaly generated by anthropogenic surfaces and human activities, i.e. the UHI, represents a significant stressor on urban ecosystems and their biota. During periods of extreme heat, UHI intensification exacerbates heatwave impacts, driving marked increases in morbidity and mortality (Jiang et al., 2019). According to a global meta-analysis by Wienert and Kuttler (Wienert and Kuttler, 2005), latitude accounted for only ~6 % of the observed variance in urban heat island magnitudes, indicating that regional land-cover and urban form exert a stronger control than meridional position on local thermal anomalies. Moreover, long-term observations reported by Varquez and

Kanda (2018) reveal a gradual annual increase in SUHI intensity on the order of 0.5–1.1 °C per century, underscoring the compounding effects of climate warming and urbanization. As global temperatures continue to rise and urban populations expand, both the frequency and severity of heatwaves, and, thus, populations' exposure to elevated thermal stress, are projected to grow, underscoring the urgent need for mitigation strategies in city planning and ecosystem management (Mentaschi et al., 2022). An increasing number of studies at different scales have been implemented to meet this need (Parastatidis et al., 2017; Almeida et al., 2021). Parastatidis et al. (2017) developed LST products for the globe based on Landsat 5, 7 and 8 through Google Earth Engine (GEE). Some tools were implemented to map UHI across different cities, e.g. by Climate Central, and by OKI although both are available only for a limited number of U.S. cities. Several exemplar cities have voluntarily implemented initiatives and projects, e.g. Los Angeles, Singapore, Barcelona, Beijing, Milan exploring different strategies to mitigate the UHI phenomenon. A notable initiative is C40 Cities, an ongoing database of city heat-mitigation actions and best practices, among other topics covered. The UHI phenomenon is gaining prominence on the agendas of urban planners, yet there remains a shortage of practical, widely accessible and dynamic tools to effectively address the challenge. Beyond global analyses and city-scale initiatives, concrete experiences of data sharing and participatory engagement further illustrate how UHI knowledge can be operationalized in practice. At a local scale, the workflow was piloted in Bologna's Pescarola district during a community assembly in May 2025. On this occasion, scientists presented maps generated through the workflow and later organized a participatory bicycle survey using thermal mobile sensors (Barbano et al., 2024) to collect fine-grained environmental data in different parts of the cities, from highly urbanized to green urban areas, highlighting the Pescarola district as one of the main cooling area of the city of Bologna, and supported the need to preserve this area from urbanization. If embedded within municipal infrastructures, the workflow could be widely adopted by local committees and communities, fostering active engagement with spatial data and creating new opportunities for dialogue between citizens and experts. Such initiatives align with the idea of democratizing science, which emphasizes not only open access but also the proactive involvement of both researchers and communities in co-producing knowledge and shaping urban-climate strategies.

7.2. Advancing SDGs

The relevance of this study extends beyond technical innovation, as it actively contributes to multiple dimensions of sustainable development. By enabling accessible, scalable, and inclusive assessments of urban thermal anomalies, the proposed workflow supports the achievement of key United Nations Sustainable Development Goals (SDGs) (United Nations, 2015).

SDG 3 – Good Health and Well-being. The proposed workflow enhances the capacity to identify and visualize urban thermal anomalies, which are increasingly linked to public health risks such as heat stress, cardiovascular strain, and respiratory distress (Ballester et al., 2023; Yadav et al., 2023). By making SUHII maps accessible to local authorities, urban planners, and even non-experts, the platform supports early identification of heat-vulnerable areas, (Voelkel et al., 2018; Meenar et al., 2023). This geospatial evidence can inform targeted health interventions, guide the distribution of cooling infrastructure, and ultimately support efforts to reduce environmental determinants of ill health in urban settings (Avtar et al., 2020). While the current workflow produces spatially explicit maps of SUHII, its ability to support climate justice would be substantially enhanced by coupling these outputs with demographic layers. This would allow identification of heat-vulnerable areas where socio-economically marginalized populations are disproportionately exposed to thermal stress. Such integration is a key step for informing targeted mitigation and adaptation measures that address both environmental and social inequities. Future implementations will aim at linking environmental data with public well-being, contributing to more holistic approaches to urban health resilience.

SDG 11 – Sustainable Cities and Communities. The proposed workflow directly advances SDG 11 by democratizing access to geospatial tools for monitoring surface urban thermal anomalies, in any city worldwide, by leveraging open data and standardized procedures. The workflow leverages globally available datasets (Landsat, SRTM, OSM) and integrates them via standardized, reproducible procedures. The outputs are ready-to-use maps, distributed in an open format. A key innovation is the integrated analysis that also considers topography, making the workflow generalizable to any city in the world, without the risk of introducing error of over- or underestimation of thermal anomaly due to comparing between rural and urban temperatures at different altitudes (Zargari et al., 2024): the algorithm automatically segments the AOI into altitudinally homogeneous areas of 100 m and estimates thermal anomalies inside each level, and then merges all the results in the final map. Ultimately, by lowering barriers to information, the platform fosters more resilient and equitable urban development in line with the goals of SDG 11 (Moreno et al., 2010).

Advancing SDG 13 – Climate Action. The workflow contributes to SDG 13 by equipping cities and citizens with a replicable, scalable tool to understand and respond to local manifestations of climate change (Yuan, 2021). SUHII is a key indicator of climate-related stress in cities, closely tied to human health, energy demand, and ecosystem degradation. The algorithm's core processing logic is efficient, since the LST derivation takes about 17 s, the thermal anomaly and SUHII calculation about 1.68 min, and the distance from GUA measure is near-instantaneous. The efficient processing logic, capable of deriving LST in under 20 min in most cases, makes the tool suitable for widespread adoption, including in data- or resource-constrained settings. Also, DEM download and handling are efficient. The main bottlenecks are the Landsat and OSM data download, that together account for about 90 % of total processing time. Similarly, peak memory usage, up to ~27 GB in the largest cases, could limit reproducibility on moderate-RAM systems. To improve performance and robustness, future implementations should prioritize caching or pre-clipping data requests, overlap downloads with compute via parallel task scheduling, and adopt tile-based or streaming approaches to lower peak memory demands. Targeting these I/O and memory-bound steps has the greatest potential to reduce average runtimes below 20 min and stabilize processing across heterogeneous urban areas.

The entire workflow, from data acquisition and preprocessing to integration, has been fully automated, eliminating the need for specialized technical expertise and reducing manual intervention to a few simple inputs. Users supply only two parameters: AOI and local folder path, and the system produces SUHII maps that are delivered locally and rendered within a coherent thematic framework. By democratizing access to SUHI analyses, this platform enables non-expert stakeholders to visualize SUHI dynamics, raises awareness of urban-climate interactions, and catalyses more informed decision-making (Verhegghen et al., 2021). Moreover, it serves as a bridge between citizens, including marginalized communities, policy makers, and urban planners, fostering collaborative, evidence-based strategies for urban climate adaptation and justice (Nagaraj et al., 2020; Bennett et al., 2022; Brett, 2022). At the level of policymakers, the proposed approach ensures both inter- and intra-urban scalability: it allows comparison of heat adaptation policies between different cities and at the same time maps individual SUHIs within each, facilitating the identification of the most effective strategies and areas requiring improvement. Planned future extensions, such as time series analysis and predictive modelling, will further support anticipatory adaptation strategies. By visualizing urban thermal patterns in space and time, the workflow promotes data-driven climate action that is locally grounded but globally coherent. This includes identifying heat-vulnerable areas, evaluating the impact of green infrastructure, and informing heat mitigation measures. Moreover, the standardized and open nature of the methodology

supports transparency and repeatability, foundational principles for tracking progress under international climate agreements. In this way, the platform helps translate global climate goals into concrete, place-based actions that align with the priorities of SDG 13.

Advancing SDG 16 – Peace, Justice and Strong Institutions. By promoting transparency, accountability, and public access to environmental data, the workflow supports inclusive governance and strengthens the interface between citizens and institutions (Avtar et al., 2020). It reduces reliance on technical gatekeeping and supports community-led data interpretation and advocacy. The standardized nature of the outputs ensures that all stakeholders, regardless of institutional capacity, have access to the same information, helping to level the playing field in urban climate negotiations. In contexts where environmental injustice and institutional opacity prevail, such tools can support more equitable participation in urban development processes and reinforce institutional trust through open, verifiable evidence.

Advancing SDG 17 – Partnerships for the Goals. Finally, the project aligns with SDG 17 by fostering open, cross-sectoral collaboration through open science principles (Bachmann et al., 2022). By releasing the workflow under the GNU General Public License v3.0 (GPL 3.0) and providing implementations in both R and Python, the project promotes inclusivity in technical development and downstream use.

This framework explicitly permits any user, including academic researchers, professional firms, NGOs, and other stakeholders, to use the data or derivatives thereof, provided that appropriate credit is given. This approach encourages broad dissemination, independent verification, and value-added applications across both public and private sectors (Nagaraj et al., 2020). The workflow code, available in both R and Python, is openly hosted on GitHub. This multi-language, modular design not only fosters collaborative development and rapid evolution by researchers and stakeholders but also enables seamless integration of new data sources and functionalities. By leveraging community-driven peer-review and extensions, the codebase remains robust, extensible, and easily maintainable over time. This solid framework is enclosed in a script, which will also be made accessible through a user-friendly web platform and a QGIS plugin. This open, participatory framework embodies the principles of SDG 17 by strengthening the global science-policy interface and enabling co-creation of solutions to shared urban and climate challenges. The workflow directly aims at being a tool for grassroots engagement when placed in the hands of communities. A first example of this potential was demonstrated in Bologna's Pescarola district, where maps generated with the workflow were presented to citizens and complemented by a participatory bicycle survey with mobile sensors (Fig. 4). This experience helped residents to recognize how specific green areas in their neighbourhood contribute to mitigating the local heat island effect, fostering both awareness and collective agency. In this way, the workflow acts not only as a scientific instrument but also as an enabler of participatory governance, allowing communities to highlight local vulnerabilities, advocate for interventions, and co-design solutions.

7.3. Limitations and future developments

Despite its strengths, the methodology has inherent limitations. Persistent cloud cover can obscure land surface signals, leading to temporal gaps or biases in SUHII retrievals (Mirzaei and Haghighat, 2010). Second, Landsat's daytime thermal overpasses mean that measured LST is strongly influenced by direct solar heating, which can obscure the underlying heat storage and re-emission processes that dominate nocturnal urban warming, hence our focus on the SUHII, i.e., skin-temperature, rather than the classical air temperature-based UHI (Mutiibwa et al., 2015). Because satellite-derived LST can exceed ambient air temperatures by several degrees under strong insolation, it is essential to emphasize that our analysis quantifies surface temperature differentials, not air-temperature anomalies. Moreover, the daytime acquisition times capture only a transient thermal snapshot: as the afternoon progresses and especially after sunset, urban materials continue to release stored heat, typically amplifying urban-rural temperature gaps at night (Zargari et al., 2024). Thus, SUHII maps based on midday imagery should be interpreted with caution, acknowledging both the diurnal variability of surface heat patterns and the fundamental differences between LST and air temperatures. Looking ahead, integrating nighttime LST is essential to characterize the cycle of urban heat storage and release. While Landsat nighttime coverage is sparse, fusing its high spatial detail with more frequent thermal missions (e.g., ECOSTRESS, Sentinel-3, VIIRS and other suitable sensors) can produce both high-temporal and spatial resolution composites, SUHII amplitude metrics, and simple diurnal models constrained by surface energy-balance considerations. Such integration would better capture the nocturnal intensification that is most relevant for heat-stress exposure. Finally, spatial resolution in thermal sensors, such as Landsat's 30 m thermal resolution averages the signal over mixed surfaces, effectively "smoothing out" fine-scale heterogeneity in urban landscapes. As a result, small but intense heat hotspots, such as paved plazas,

Fig. 4. Public assembly in Pescarola (Bologna, Italy) and participatory bicycle surveys.

dark rooftops, or narrow street canyons, are diluted by adjacent cooler areas, leading to a systematic underestimation of peak SUHII intensities (Kim and Brown, 2021). While the smoothing effect of 30 m resolution may underestimate extreme temperatures at the scale of a single rooftop or small paved area, for urban planning purposes the aggregation of thermal accumulator surfaces (e.g., blocks of impervious areas, clusters of buildings) is often more relevant than isolated hotspots. Planning interventions typically target neighbourhood or district scales, where Landsat-derived patterns remain highly informative for prioritizing mitigation strategies. At the same time, finer-scale planning decisions can be addressed using complementary tools, including UAV-based thermal surveys, building-level simulations, or very high–resolution (VHR) imagery. These considerations should guide both the use and further refinement of the platform. Another limitation of the present workflow is the absence of a formal uncertainty budget for SUHII and of error-propagation from the underlying datasets. Landsat LST carries retrieval uncertainty stemming from atmospheric correction, emissivity assumptions, and cross-sensor harmonization, that can propagate into SUHII. Additional bias may arise from OSM incompleteness or positional error, which can misclassify urban vs. rural pixels and systematically shift SUHII, as well as from DEM quality and resampling, which affect terrain correction and thus LST in complex topography. Future versions should quantify uncertainty at per-pixel or zone-level standard errors/credible intervals. Reporting city-level confidence intervals and robustness ranges, alongside maps of uncertainty, would allow readers to distinguish signal from noise and to judge when differences between cities or seasons are statistically meaningful. Until such analyses are included, SUHII magnitudes should be interpreted as indicative rather than exact, and cross-site rankings treated with caution.

Validation of SUHII is intrinsically challenging because a suitable “truth” for radiometric LST at Landsat scales is rarely available. Near-surface air temperature (typically measured at ~2 m) is a different physical quantity than LST and often decouples from the surface, especially under strong insolation, low wind, or heterogeneous urban materials, so agreement with air temperature cannot be interpreted as validation of LST or SUHII. Point radiometers and flux towers provide surface-focused measurements, but they sample micro-environments, differ in view geometry and timing from satellite overpasses, and may not represent the within-pixel heterogeneity of 30 m urban scenes. Cross-comparison with other satellite LST products (e.g., MODIS, ECOSTRESS, Sentinel-3) can flag gross inconsistencies but does not establish truth because products share retrieval assumptions and may exhibit correlated errors; consequently, inter-product agreement is not sufficient evidence of accuracy. Regarding the newly proposed 100m-bending approach to map thermal anomalies, validation results support its robustness. Matsumoto is the only site where the banded approach departs slightly from the lapse-corrected reference. Its narrow, steep basin promotes non-linear elevation-LST behavior (cold-air pooling, strong aspect effects), so 100-m bands mix pixels with very different radiative conditions. In several bands the rural sample is sparse and topographically biased toward sunlit slopes, elevating the rural reference and compressing SUHII dynamics. Mitigations include enforcing larger rural pixel counts or adaptive band widths, stratifying rural means by aspect/hillshade (or using medians), and tightening alignment checks. Finally, to move beyond SUHII and map the air-temperature UHI itself, the workflow should assimilate observations from urban meteorological networks (WMO stations, municipal/academic arrays) and vetted crowdsourced sensors. The outcome would be co-produced LST-based indicators and air-temperature UHI maps, with quantified uncertainty, that are more directly actionable for public health and urban planning. The application is a contribution in the framework of critical remote sensing and data democratization, to make more ethical and socially available the commons of satellites information (Segarra et al., 2024). As exposed in the six steps of the framework of Bennett et al. (2024), this tool emphasizes empowerment and accessibility. In this sense another possible limitation to be acknowledged relates to the technological resource’s availability: the application of multi-temporal classification algorithms over extended time series requires computational power and data storage. Access to adequate hardware and stable data connections can therefore become a limiting factor, particularly when analyses are conducted in settings where such infrastructure is not readily available.

8. Conclusions

The developed workflow demonstrates that Surface Urban Heat Island Intensity (SUHII) analysis can be made accessible, reproducible, and actionable through a user-friendly, automated, and modular approach. By minimizing the need for technical expertise, the platform opens opportunities for broader participation, supporting inclusive knowledge production and fostering climate awareness on the local scale. This accessibility promotes engagement across sectors, from scientific research to community advocacy, and reinforces the value of Earth Observation data as a public good. The architecture of the platform supports rapid adaptation to evolving data sources and user needs, highlighting its potential for long-term scalability and replicability in diverse urban contexts. While the current implementation delivers consistent and spatially detailed SUHII products, the integration of time series analysis and predictive models represents a key opportunity to move toward anticipatory frameworks for urban climate resilience. Similarly, the enrichment of the workflow with socio-economic, demographic, and infrastructural data would allow the transition from thermal anomaly mapping to multidimensional urban risk assessments. The results point to a broader principle: accessible, modular geospatial workflows can serve as a foundation for bridging the gap between environmental monitoring and policy implementation. By aligning with the SDGs, particularly SDGs 3, 11, 13, 16 and

17, this work contributes to the advancement of equitable climate adaptation strategies and urban environmental health justice. The platform fosters citizen empowerment and supports data-informed decision-making, offering a replicable model for cities aiming to understand and address the impacts of climate change on human health, well-being, and social equity.

Code Availability

The workflow code is available on GitHub at https://github.com/Officina-SCIFT/SUHII_mapping.

CRediT authorship contribution statement

Giovanni Marco De Pieri: Writing – review & editing, Resources, Project administration. **Christopher Ceresi:** Writing – review & editing, Resources, Project administration. **Federico Baldo:** Writing – review & editing, Software, Methodology. **Matteo Francobaldi:** Writing – review & editing, Software, Methodology. **Salvatore Eugenio Pappalardo:** Writing – review & editing, Writing – original draft, Supervision, Resources, Project administration. **Chiara Richiardi:** Writing – review & editing, Writing – original draft, Visualization, Validation, Software, Methodology, Formal analysis, Data curation, Conceptualization. **Letizia Caroscio:** Writing – review & editing, Visualization, Project administration, Methodology, Investigation, Conceptualization. **Edoardo Crescini:** Writing – review & editing, Project administration, Investigation. **Massimo De Marchi:** Writing – review & editing, Supervision.

Declaration of Competing Interest

The authors declare that they have no known competing financial interests or personal relationships that could have appeared to influence the work reported in this paper.

Acknowledgements

We sincerely thank the editor and reviewers for their thoughtful and constructive comments, which substantially enhanced the rigor of the workflow and the clarity of the manuscript. We also extend our heartfelt thanks to the entire *Municipi Sociali* community of Bologna, Làbas, TPO, and Offside, not only for bringing us together, but for embodying the values of citizen science, collective action, and social commitment. Their support and vision remind us that scientific work can be a meaningful contribution to a better world, one grounded in climate justice and community empowerment. We also thank the organizations *Codici* and *ÈNostra* for their essential support in activating this project, for believing in it and standing by us throughout its development.

Appendix A. Supporting information

Supplementary data associated with this article can be found in the online version at doi:10.1016/j.susgeo.2025.100006.

Data availability

The data that support the findings of this study and the workflow code are openly available in GitHub at https://github.com/Officina-SCIFT/SUHII_mapping.

References

Al Echcheikh El Alaoui, D., 2025. Architectural and planning adaptations of historical urban landscapes: from traditional medinas to sustainable streets in hot climates. Curr. Probl. Archit. Urban Plan. (71), 264–273. https://doi.org/10.32347/2077-3455.2025.71.264-273.

Almeida, C.R., de, Teodoro, A.C., Gonçalves, A., 2021. Study of the Urban Heat Island (UHI) using remote sensing data/techniques: a systematic review. Environments 8 (10), 105. https://doi.org/10.3390/environments8100105.

Anguelovski, I., Kotsila, P., Lees, L., Triguero-Mas, M., Calderón-Argelich, A., 2024. From heat racism and heat gentrification to urban heat justice in the USA and Europe. Nat. Cities 2 (1), 8–16. https://doi.org/10.1038/s44284-024-00179-6.

Avtar, R., Aggarwal, R., Kharrazi, A., Kumar, P., Kurniawan, T.A., 2020. Utilizing geospatial information to implement SDGs and monitor their Progress. In: Environmental Monitoring and Assessment, 192. Springer. https://doi.org/10.1007/s10661-019-7996-9.

Bachmann, N., Tripathi, S., Brunner, M., Jodlbauer, H., 2022. The Contribution of Data-Driven Technologies in Achieving the Sustainable Development Goals. Sustainability 14 (5), 2497. https://doi.org/10.3390/su14052497.

Ballester, J., Quijal-Zamorano, M., Méndez Turrubiates, R.F., Pegenaute, F., Herrmann, F.R., Robine, J.M., Basagaña, X., Tonne, C., Antó, J.M., Achebak, H., 2023. Heat-related mortality in Europe during the summer of 2022. Nat. Med. 29 (7), 1857–1866. https://doi.org/10.1038/s41591-023-02419-z.

Bara, M. (2025). Accessibility Barriers in Multi-Terabyte Public Datasets: The Gap Between Promise and Practice. ⟨http://arxiv.org/abs/2506.13256⟩.

Barbano, F., Brattich, E., Cintolesi, C., Ghafoor Nizamani, A., Di Sabatino, S., Milelli, M., Peerlings, E.E.M., Polder, S., Steeneveld, G.-J., Parodi, A., 2024. Performance evaluation of MeteoTracker mobile sensor for outdoor applications. Atmos. Meas. Tech. 17 (10), 3255–3278. https://doi.org/10.5194/amt-17-3255-2024.

Bennett, M.M., Chen, J.K., Alvarez León, L.F., Gleason, C.J., 2022. The politics of pixels: a review and agenda for critical remote sensing. Prog. Hum. Geogr. 46 (3), 729–752. https://doi.org/10.1177/03091325221074691.

Bennett, M.M., Gleason, C.J., Tellman, B., Alvarez Leon, L.F., Friedrich, H.K., Ovienmhada, U., Mathews, A.J., 2024. Bringing satellites down to Earth: six steps to more ethical remote sensing. Glob. Environ. Change Adv. 2, 100003. https://doi.org/10.1016/j.gecadv.2023.100003.

Brett, A., 2022. Information as Power: democratizing environmental data. SSRN Electron. J. https://doi.org/10.2139/ssrn.4058461.

Bulkeley, H., Carmin, J., Castán Broto, V., Edwards, G.A.S., Fuller, S., 2013. Climate justice and global cities: mapping the emerging discourses. Glob. Environ. Change 23 (5), 914–925. https://doi.org/10.1016/j.gloenvcha.2013.05.010.

Bulkeley, H., Edwards, G.A.S., Fuller, S., 2014. Contesting climate justice in the city: examining politics and practice in urban climate change experiments. Glob. Environ. Change 25, 31–40. https://doi.org/10.1016/j.gloenvcha.2014.01.009.

Cañizares, J.C., Copeland, S., Doorn, N., 2024. Embedding justice considerations in climate resilience. Ethics Policy Environ. 27 (1), 63–88. https://doi.org/10.1080/21550085.2023.2197824.

Charpentier, M.A., Groffman, P.M., 1992. Soil moisture variability within remote sensing pixels. J. Geophys. Res. Atmospheres 97 (D17), 18987–18995. https://doi.org/10.1029/92JD00882.

Earth Resources Observation and Science (EROS) Center. (2020). Landsat 8-9 Operational Land Imager / Thermal Infrared Sensor Level-2, Collection 2. U.S. Geological Survey.

Earth Resources Observation and Science (EROS) Center. (2024). Landsat 8-9 Collection 2 (C2) Level 2 Science Product (L2SP) Guide.

Eyni, A., Zaitchik, B.F., Hobbs, B.F., Hadjimichael, A., Shi, R., 2025. Distributional outcomes of urban heat island reduction pathways under climate extremes. Sci. Rep. 15 (1), 9594. https://doi.org/10.1038/s41598-025-93896-4.

Gardiner, S.M., 2011. Climate Justice. Oxford University Press. https://doi.org/10.1093/oxfordhb/9780199566600.003.0021.

Grislain-Letrémy, C., Sixou, J., Sotura, A., 2025. Urban heat islands and income inequalities: evidence from French cities. Ecol. Econ. 235, 108624. https://doi.org/10.1016/j.ecolecon.2025.108624.

Ho, H.C., Tong, S., Zhou, Y., Hu, K., Yang, X., Yang, Y., 2025. Mapping heat vulnerability and heat risk for neighborhood health risk management in urban environment? challenges and opportunities. Curr. Environ. Health Rep. 12 (1), 14. https://doi.org/10.1007/s40572-025-00478-7.

Javanroodi, K., Nik, V.M., Scartezzini, J.L., 2021. Quantifying the impacts of urban morphology on modifying microclimate conditions in extreme weather conditions. J. Phys. Conf. Ser. 2042 (1), 012058. https://doi.org/10.1088/1742-6596/2042/1/012058.

Javanroodi, K., Nik, V.M., Giometto, M.G., Scartezzini, J.-L., 2022. Combining computational fluid dynamics and neural networks to characterize microclimate extremes: learning the complex interactions between meso-climate and urban morphology. Sci. Total Environ. 829, 154223. https://doi.org/10.1016/j.scitotenv.2022.154223.

Jiang, S., Lee, X., Wang, J., Wang, K., 2019. Amplified Urban Heat Islands during Heat Wave Periods. J. Geophys. Res. Atmos. 124 (14), 7797–7812. https://doi.org/10.1029/2018JD030230.

Kim, Y., 2023. Accessibility and contribution limitations of authoritative climate information: evaluating the usability and inclusivity of IPCC's website. Tech. Commun. Soc. Justice 1 (1), 24–40. ⟨https://techcommsocialjustice.org/index.php/tcsj/article/view/18⟩.

Kim, S.W., Brown, R.D., 2021. Urban heat island (UHI) variations within a city boundary: a systematic literature review. Renew. Sustain. Energy Rev. 148, 111256. https://doi.org/10.1016/J.RSER.2021.111256.

Knott, J.A., Liknes, G.C., Giebink, C.L., Oh, S., Domke, G.M., McRoberts, R.E., Quirino, V. F., Walters, B.F., 2023. Effects of outliers on remote sensing-assisted forest biomass estimation: a case study from the United States national forest inventory. Methods Ecol. Evol. 14 (7), 1587–1602. https://doi.org/10.1111/2041-210X.14084.

Kumar, S., Imen, S., Sridharan, V.K., Gupta, A., McDonald, W., Ramirez-Avila, J.J., Abdul-Aziz, O.I., Talchabhadel, R., Gao, H., Quinn, N.W.T., Weiss, W.J., Poulose, T., Palmate, S.S., Lee, C.M., Baskaran, L., 2024. Perceived barriers and advances in integrating earth observations with water resources modeling. Remote Sens. Appl. Soc. Environ. 33, 101119. https://doi.org/10.1016/j.rsase.2023.101119.

Lauwaet, D., Berckmans, J., Hooyberghs, H., Wouters, H., Driesen, G., Lefebre, F., De Ridder, K., 2024. High resolution modelling of the urban heat island of 100 European cities. Urban Clim. 54, 101850. https://doi.org/10.1016/j.uclim.2024.101850.

Li, Z., Shen, H., Weng, Q., Zhang, Y., Dou, P., Zhang, L., 2022. Cloud and cloud shadow detection for optical satellite imagery: features, algorithms, validation, and prospects. ISPRS J. Photogramm. Remote Sens. 188, 89–108. https://doi.org/10.1016/j.isprsjprs.2022.03.020.

Meenar, M., Rahman, M.S., Russack, J., Bauer, S., Kapri, K., 2023. The urban poor and vulnerable are hit hardest by the heat": a heat equity lens to understand community perceptions of climate change, urban heat islands, and green infrastructure. Land 12 (12), 2174. https://doi.org/10.3390/land12122174.

Mentaschi, L., Duveiller, G., Zulian, G., Corbane, C., Pesaresi, M., Maes, J., Stocchino, A., Feyen, L., 2022. Global long-term mapping of surface temperature shows intensified intra-city urban heat island extremes. Glob. Environ. Change 72, 102441. https://doi.org/10.1016/J.GLOENVCHA.2021.102441.

Mirzaei, P.A., Haghighat, F., 2010. Approaches to study Urban Heat Island – abilities and limitations. Build. Environ. 45 (10), 2192–2201. https://doi.org/10.1016/j.buildenv.2010.04.001.

Moreno, E.L., Oyeyinka, O., Mboup, G., 2010. State of the world's cities 2010/2011. Bridg. Urban Divid.

Mutiibwa, D., Strachan, S., Albright, T., 2015. Land surface temperature and surface air temperature in complex terrain. IEEE J. Sel. Top. Appl. Earth Obs. Remote Sens. 8 (10), 4762–4774. https://doi.org/10.1109/JSTARS.2015.2468594.

Nagaraj, A., Shears, E., De Vaan, M., 2020. Improv. Data Access Democr. Divers. Sci. 117, 23490–23498. https://doi.org/10.1073/pnas.2001682117/-/DCSupplemental.y.

Nieuwenhuijsen, M.J., Dadvand, P., Márquez, S., Bartoll, X., Barboza, E.P., Cirach, M., Borrell, C., Zijlema, W.L., 2022. The evaluation of the 3-30-300 green space rule and mental health. Environ. Res. 215, 114387. https://doi.org/10.1016/j.envres.2022.114387.

Oke, T.R., 1973. City size and the urban heat island. Atmos. Environ. 7 (8), 769–779. https://doi.org/10.1016/0004-6981(73)90140-6.

OpenStreetMap contributors. (2025). OpenStreetMap. In Available as Open Data under the Open Data Commons Open Database License (ODbL) at ⟨http://openstreetmap.org/⟩. OpenStreetMap Foundation.

Pappalardo, E.S., Zanetti, C., Todeschi, V., 2023. Mapping urban heat islands and heat-related risk during heat waves from a climate justice perspective: a case study in the municipality of Padua (Italy) for inclusive adaptation policies. Landsc. Urban Plan. 238, 104831. https://doi.org/10.1016/j.landurbplan.2023.104831.

Parastatidis, D., Mitraka, Z., Chrysoulakis, N., Abrams, M., 2017. Online global land surface temperature estimation from landsat. Remote Sens. 9 (12), 1208. https://doi.org/10.3390/rs9121208.

Porter, L., Rickards, L., Verlie, B., Bosomworth, K., Moloney, S., Lay, B., Latham, B., Anguelovski, I., Pellow, D., 2020. Climate justice in a climate changed world. Plan. Theory Pract. 21 (2), 293–321. https://doi.org/10.1080/14649357.2020.1748959.

R core team. (2024). R: A Language and Environment for Statistical Computing. In ⟨https://www.R-project.org/⟩. R Foundation for Statistical Computing.

Rigon, A., 2025. Claiming a role for planning in intersectional climate justice. Cities 166, 106194. https://doi.org/10.1016/j.cities.2025.106194.

Robinson, M., Shine, T., 2018. Achieving a climate justice pathway to 1.5 °C. Nat. Clim. Change 8 (7), 564–569. https://doi.org/10.1038/s41558-018-0189-7.

Roshan, G., Arekhi, S., Bayganeh, Z., Attia, S., 2024. Evaluation of the intensity of urban heat islands during heat waves using local climate zones in the semi-arid, continental climate of Tehran. Urban Clim. 56, 102079. https://doi.org/10.1016/j.uclim.2024.102079.

Rubel, F., Kottek, M., 2010. Observed and projected climate shifts 1901-2100 depicted by world maps of the Köppen-Geiger climate classification. Meteorol. Z. 19 (2), 135–141. https://doi.org/10.1127/0941-2948/2010/0430.

Ruiz de Gopegui, M., Olazabal, M., Castán Broto, V., McPhearson, T., 2025. Climate justice in urban public space adaptation: developing and testing a collective assessment tool in Hunters Point, New York City. Urban Clim. 62, 102505. https://doi.org/10.1016/j.uclim.2025.102505.

Ruosteenoja, K., Jylhä, K., 2023. Average and extreme heatwaves in Europe at 0.5–2.0 °C global warming levels in CMIP6 model simulations. Clim. Dyn. 61 (9–10), 4259–4281. https://doi.org/10.1007/s00382-023-06798-4.

Santamouris, M., 2020. Recent progress on urban overheating and heat island research. Integrated assessment of the energy, environmental, vulnerability and health impact. Synergies with the global climate change. Energy Build. 207, 109482. https://doi.org/10.1016/j.enbuild.2019.109482.

Segarra, J., González-Fernández, A., Osorno-Covarrubias, J., Couturier, S., 2024. The role of critical remote sensing in environmental justice struggles. Prog. Environ. Geogr. https://doi.org/10.1177/27539687241269331.

Soden, R., Agrawaal, T.S., Lord, A., Chanen, C., Flawn, L., Seaifan, Z., Classens, M., Easterbrook, S., 2025. Climate data practices: a research approach for HCI and climate justice. ACM Trans. Comput. Hum. Interact. https://doi.org/10.1145/3719346.

Stewart, I.D., Mills, G., 2021. The Urban Heat Island. Elsevier. https://doi.org/10.1016/C2017-0-02872-0.

Stone, B., Hess, J.J., Frumkin, H., 2010. Urban form and extreme heat events: are sprawling cities more vulnerable to climate change than compact cities? Environ. Health Perspect. 118 (10), 1425–1428. https://doi.org/10.1289/ehp.0901879.

Stracqualursi, A., 2025. Climate adaptivity of urban form: an evaluation by the case study of Medina of Fès. J. Build. Perform. Simul. 18 (3), 351–370. https://doi.org/10.1080/19401493.2023.2251935.

United Nations. (2015). Transforming our World: the 2030 Agenda for Sustainable Development. A/RES/70/1. ⟨https://sdgs.un.org/publications/transforming-our-world-2030-agenda-sustainable-development-17981⟩.

Varquez, A.C.G., Kanda, M., 2018. Global urban climatology: a meta-analysis of air temperature trends (1960–2009). npj Clim. Atmos. Sci. 1 (1), 32. https://doi.org/10.1038/s41612-018-0042-8.

Verhegghen, A., Beauchamp, E., Seigneret, A., 2021. Democratizing Earth Observation to Improve Transparency in Land Use Governance..

Voelkel, J., Hellman, D., Sakuma, R., Shandas, V., 2018. Assessing Vulnerability to Urban Heat: A Study of Disproportionate Heat Exposure and Access to Refuge by Socio-Demographic Status in Portland, Oregon. Int. J. Environ. Res. Public Health 15 (4), 640. https://doi.org/10.3390/ijerph15040640.

Wienert, U., Kuttler, W., 2005. The dependence of the urban heat island intensity on latitude A statistical approach. Meteorol. Z. 14 (5), 677–686. https://doi.org/10.1127/0941-2948/2005/0069.

WMO. (2022). Provisional State of the Global Climate 2022.

Yadav, N., Rajendra, K., Awasthi, A., Singh, C., 2023. Systematic exploration of heat wave impact on mortality and urban heat island: A review from 2000 to 2022. Urban Clim. 51, 101622. https://doi.org/10.1016/J.UCLIM.2023.101622.

Yang, Y., Li, P., Nath, A.J., Feng, Z., Xiao, Z., Yang, J., 2025. Landsat scene- and pixel-based cloud cover research: a review. Int. J. Digit. Earth 18 (1). https://doi.org/10.1080/17538947.2025.2489732.

Yuan, M., 2021. Geographical information science for the United Nations' 2030 agenda for sustainable development. In: In International Journal of Geographical Information Science, 35. Taylor and Francis Ltd, pp. 1–8. https://doi.org/10.1080/13658816.2020.1766244.

Zargari, M., Mofidi, A., Entezari, A., Baaghideh, M., 2024. Climatic comparison of surface urban heat island using satellite remote sensing in Tehran and suburbs. Sci. Rep. 14 (1). https://doi.org/10.1038/s41598-023-50757-2.

Zhang, C., Li, G., Cui, W., 2018. High-Resolution Remote Sensing Image Change Detection by Statistical-Object-Based Method. IEEE J. Sel. Top. Appl. Earth Obs. Remote Sens. 11 (7), 2440–2447. https://doi.org/10.1109/JSTARS.2018.2817121.

Zhou, D., Xiao, J., Bonafoni, S., Berger, C., Deilami, K., Zhou, Y., Frolking, S., Yao, R., Qiao, Z., Sobrino, J.A., 2018. Satellite remote sensing of surface urban heat islands: progress, challenges, and perspectives. Remote Sens. 11 (1), 48. https://doi.org/10.3390/rs11010048.